Anisotropic suppression of hyperuniformity of elastic systems in media with planar disorder

Joaquín Puig,[1] Federico Elías,[1] Jazmín Aragón Sánchez,[1] Raúl Cortés Maldonado,[1] Gonzalo Rumi,[1] Gladys Nieva,[1] Pablo Pedrazzini,[1] Alejandro B. Kolton,[1] and Yanina Fasano*[1]

[1] *Centro Atómico Bariloche and Instituto Balseiro, CNEA, CONICET and Universidad Nacional de Cuyo, Avenida Bustillo 9500, 8400 San Carlos de Bariloche, Argentina*

(Dated: May 3, 2022)

arXiv:2205.00437v1 [cond-mat.supr-con] 1 May 2022

Abstract

Disordered hyperuniform materials with vanishing long-wavelength density fluctuations are attracting attention due to their unique physical properties. In these systems, the large-scale density fluctuations are strongly suppressed as in a perfect crystal, even though the system can be disordered like a liquid. Yet, hyperuniformity can be affected by the different types of quenched disorder unavoidably present in the host medium where constituents are nucleated. Here, we use vortex matter in superconductors as a model elastic system to study how planar correlated disorder impacts the otherwise hyperuniform structure nucleated in samples with weak point disorder. Planes of defects suppress hyperuniformity in an anisotropic fashion: While in the transverse direction to defects the long-wavelength density fluctuations are non-vanishing, in the longitudinal direction they are smaller and the system can eventually recover hyperuniformity for sufficiently thick samples. Our findings stress the need of considering the nature of disorder and thickness-dependent dimensional crossovers in the search for novel hyperuniform materials.

* Corresponding author: Yanina.Fasano@cab.cnea.gov.ar

PACS numbers:

Introduction

A great number of disordered physical and biological systems are endowed with a universal hidden order characterized by a macroscopically uniform density of constituents.[1,2] This hidden order is the structural property of hyperuniformity, characterized by an anomalous suppression of large-scale density fluctuations in the system. This property is naturally expected in a crystal, but it is also observed in a wide variety of disordered systems such as two-dimensional material structures,[3–8] jammed particles,[9,10] bubbles in foam,[11] vortex matter in type-II superconductors,[12,13] patterns of photoreceptors in avian retinas,[14] biological tissues,[15] and even the distribution of the density fluctuations in the early Universe.[16] Hyperuniform systems present a vanishing structure factor in the infinite-wavelength or small wavenumber q limit, namely $S(\mathbf{q}) \to 0$ as $\mathbf{q} \to \mathbf{0}$.[1,2] This magnitude can be directly measured via different diffraction techniques and provides information on the fluctuations of the density of constituents of the system at different wavenumbers. Since hyperuniformity is a property defined in an asymptotic limit, strict hyperuniformity is difficult to ascertain in experimental as well as computer-simulated systems. Then, most works show that the systems are effectively hyperuniform.[17]

This exceptional but ubiquitous state of matter presents a phenomenology that goes against the conventional wisdom on the effect of disorder in the physical properties of systems of interacting objects.[2–4] For instance, disorder typically lowers the electrical conductivity of metallic materials. However, a recent work reports that disordered hyperuniform systems present a closing of bandgaps resulting in an enhanced conductivity.[5] Also, periodic or quasiperiodic order was assumed as a prerequisite for a material to present photonic bandgap properties. Strikingly, disordered hyperuniform-engineered materials possess complete photonic bandgaps blocking all directions and polarizations for short wavelengths.[3,18,19] In addition, hyperuniform patterns can be very useful in practical technological applications. For example, hyperuniform patterns of defects can pin with high efficiency the vortex structure nucleated in superconductors, avoiding the undesirable dissipation that can occur in superconducting devices.[20,21]

Theoretically, due to the fluctuation-compressibility theorem, hyperuniformity may naturally emerge at thermal equilibrium in incompressible systems with long-range repulsive interactions between the constituents.[2] Nevertheless, a hyperuniform point pattern within a higher dimensional system presenting only short-range interactions or gradient terms at equilibrium may also exist. Indeed, a three dimensional vortex lattice model with short-range repulsions and local elasticity may present hyperuniform two-dimensional point patterns at every plane perpendicular to the vortex lines.[12] In general terms, this road to hyperuniformity results from bulk-mediated effective long-range interactions between the points in the hyperuniform pattern.

Vortex matter in superconductors is a model system to study the occurrence of hyperuniformity in media with different types of disorder. Vortices are elastic objects

that nucleate in type-II superconductors when applying a magnetic field. They are string-like zones of the material that concentrate a quantized amount of magnetic flux and interact repulsively between each other. The competition between this repulsion and the pressure exerted by the field results in vortices forming a structure with lattice spacing $a \propto B^{-1/2}$. The vortex structure stabilizes in solid, glassy and liquid phases, depending on temperature, applied field, the particular material and the nature of disorder in the samples.[22–34] The nucleation of quasi-ordered and disordered hyperuniform vortex structures has first been reported experimentally in samples of the high-T_c $Bi_2Sr_2CaCu_2O_{8+\delta}$ with respectively weak point and strong columnar disorder.[12] Later, disordered hyperuniform vortex structures have been observed at high fields in several superconductors presenting weak and strong point disorder.[13] Hyperuniform vortex structures are theoretically expected for media with weak point disorder since in this case the effective interaction between vortex tips at the sample surface is long ranged. Theoretically, a suppression of hyperuniformity is expected for media with columnar correlated disorder.[12] However, in the latter case an algebraic decay of $S(\mathbf{q})$ in the $\mathbf{q} \to \mathbf{0}$ limit is detected experimentally. This apparent discrepancy between theory and experiment is quite likely due to the viscous freezing of the system when field-cooling from the hyperuniform vortex liquid phase towards the low-temperature glassy vortex phase.[12] In contrast, in the case of a type-II superconductor with planar correlated defects, strong fluctuations of the vortex density have been proposed as the fingerprint of a disordered gel of vortices.[35] Thus, the nature of disorder in the host medium plays a determinant role on the magnitude of density fluctuations, and thus their effect on the nucleation of hyperuniform materials deserves further investigation.

Here we address the question of whether planar correlated quenched disorder, even if present in a reduced region of the sample, can ultimately affect the hyperuniform hidden order. We use vortex matter in two different high-T_c superconductors as model systems. In order to be reliable, these studies on long-range vortex density fluctuations require high-resolution direct imaging of individual vortices in extended fields-of-view with thousands of vortices or more. Our experimental data with such a resolution and extension are contrasted with numerical simulations of a system of interacting elastic strings nucleated in media with planar disorder. We show that planes of crystal defects running all the way through the sample thickness produce a suppression of hyperuniformity in an anisotropic fashion. Furthermore, we discuss how finite size effects are relevant for these observations and how its removal in a sufficiently-thick sample can produce a recovery of the hyperuniform hidden order in the direction longitudinal to planar defects.

Results

Density fluctuations on large length scales in media with planar defects

A practical way to image vortex density fluctuations on large length scales is to apply the magnetic decoration technique to take snapshots of thousands of vortices at the sample surface. Magnetic decoration consists in producing nanometer-size Fe clusters that are attracted towards the local field gradient entailed by vortices on the surface of the sample.[36] We decorate vortex positions at 4.2 K after field-cooling; then the sample is warmed up to room temperature and the Fe clusters are imaged by means of scanning electron microscopy. We investigate $Bi_2Sr_2CaCu_2O_{8+\delta}$ and $YBa_2Cu_3O_7$ high-T_c superconducting samples as model media with planar correlated quenched disorder, namely domains with enhanced pinning. In the first case we study samples with few and many planar defects separating zones of the sample with slightly different orientations of their c-axis;[37,38] in the second case we consider samples with twin-boundaries that act as planar defects. For comparison, we study samples of both materials with point disorder only, namely with no planar defects as revealed by means of magnetic decoration. See Methods for further details on the experimental techniques and sample characterization.

Figure 1 shows images of the vortex structures nucleated in some of the studied samples. In the case of point disorder the structure is hexagonal whereas the planar defects induce the formation of vortex rows oriented along the direction of defects $s_\parallel$, or correspondingly $q_\parallel$ in reciprocal space. These vortex rows have generally a larger density than the average, in agreement with evidence from different imaging and dynamic techniques[37–40] that indicate that planar defects in both materials act as strong pinning centers for vortices. In $Bi_2Sr_2CaCu_2O_{8+\delta}$ samples with few planar defects, vortex rows are observed in a micron-sized region, and the hexagonal structure is recovered elsewhere, see Fig. 1 (b). The sample with many planar defects was specially chosen since most vortices are aligned in vortex rows in the whole crystal, see Figs. 1 (c) and (d). In this sample, as also reported in samples with few planar defects,[38,40] the alignment of the rows is not altered by surface steps resulting from cleaving, indicating the defects extend towards the bulk of the crystals. In the case of $YBa_2Cu_3O_7$, the structure is hexagonal in the untwinned sample and vortex rows are also observed in a heavily twinned sample, see Figs. 1 (e) and (f).

In order to characterize the vortex density fluctuations on extended fields-of-view, we analyze the structure factor $S(\mathbf{q}) \equiv S(q_x, q_y)$ from snapshots of the vortex arrangements taken at the surface of these samples. Figure 2 shows $S(\mathbf{q}) = |\hat{\rho}(q_x, q_y, z = 0)|^2$, with $\hat{\rho}$ the Fourier transform of the local vortex density modulation at the surface of the studied samples with typical thick-

ness $t \sim 5 - 30\,\mu$m.[41] A strong anisotropy is evident for samples with planar defects: Figs. 2 (b), (c) and (e) show lines of local maxima in $S(\mathbf{q})$ extended along the $q_\perp$ direction (angle $\theta = 0$) corresponding to vortex density fluctuations transversal to planar defects. At first sight, the intensity seems to faint on going towards $\mathbf{q} \to \mathbf{0}$. In the case of media with point disorder, $S(\mathbf{q})$ decays algebraically when $q \to 0$, as reported previously,[12,35] and also shown in Figs. 3 (a) and (b). We wonder whether in samples with planar defects this fainting is produced by an algebraic decay in the $\mathbf{q} \to \mathbf{0}$ limit as expected for disordered hyperuniform systems.

Figure 3 shows one of the main findings of this paper: The suppression of effective hyperuniformity induced by the addition of correlated planar disorder to the host medium. In samples with planar defects, the angularly-averaged structure factor $\langle S(q)\rangle$ for $q \to 0$ is larger than that for samples with point defects (for definition of this magnitude, see Fig. 2 (f) and Methods). More significantly, $\langle S(q)\rangle$ tends to saturate in the low-q limit. This phenomenology is observed for the two studied compounds and for crystals presenting few or many planar defects. In contrast, in samples of the same compounds but with point disorder, $\langle S(q)\rangle \sim q^\beta$ with $\beta \approx 1.2$ when $q \to 0$, a signature of effective disordered hyperuniformity.

Anisotropy in the density fluctuations on large length scales in samples with planar defects

Here we show that in samples with planar defects the suppression of hyperuniformity is anisotropic, with vortex density fluctuations of greater magnitude in the $q_\perp$ than the $q_\parallel$ direction. First, we show that the saturation of the structure factor in the $q \to 0$ limit is anisotropic for vortices nucleated in samples with planar defects. Figures 3 (c) and (d) show data of the angular structure factor $S_\theta(q)$, for different reciprocal space directions. Curves with black (white with black edge) points correspond to $S_\theta(q)$ data in the transverse direction $q_\perp$ (parallel direction $q_\parallel$), whereas color points are data for intermediate angles. Irrespective of the direction, at low q all curves tend to saturate, but while the color and white points form a pack of data around $\sim 0.02-0.03$, the black curves corresponding to the transverse modes $S_{\theta=0}(q)$ stand out and saturate at a value between 2 and 10 times larger. This is better depicted in the inserts to Fig. 3 (c) and (d). In addition, the peaks in $S_\theta(q)$ are detected at smaller q for $\theta = 0$ than for 90 degree, indicating that the average vortex spacing is smaller in the longitudinal than in the transverse direction to planar defects.

Second, in order to better characterize this anisotropy, we consider the one-dimensional structure factor of individual vortex rows that is sensitive to vortex density fluctuations along the direction of planar defects. In order to compute this magnitude, the experimental positions of vortices in individual rows are mapped in a straight line such that adjacent vortices are spaced a distance a_i and the coordinate of vortex $i+1$ is $s^\mathrm{i}_\parallel$, see the schematic representation of Fig. 4 (a). The one-dimensional structure factor of a given row is then computed as $|\hat{\rho}_1(q_\parallel)|^2$, with $\hat{\rho}_1$ the Fourier transform of the vortex density modulation along the line. Then, for each vortex row we calculate the average lattice spacing in a row, $a_\parallel \equiv \langle a_i\rangle$, and the wavenumber $q_\parallel$ is normalized by $q_{0\,\parallel} \equiv 2\pi/a_\parallel$. Finally, we average the one-dimensional structure factor over many rows to obtain the $S_1(q_\parallel)$ data shown in Fig. 4 (b). In the $q \to 0$ limit the tendency to saturation is evident: A fit of $S_1(q_\parallel) \sim q_\parallel^\beta$ yields $\beta \approx 0$ within the error for the two studied compounds.

Third, we analyze the distance-evolution of the one-dimensional displacement correlator computed along and perpendicular to the direction of defects, $W(s_\parallel)$ and $W(s_\perp)$. These magnitudes quantify the average over disorder of the displacement of vortices in the $s_\parallel$ or $s_\perp$ directions with respect to the sites of perfect chains oriented in the same directions. The lattice spacing of the perfect chains, either $a_\parallel$ or $a_\perp$, are obtained by averaging the separation of vortices along the considered direction in a given row/lane of vortices, see the schematics in the inserts to Figs. 4 (c) and (d). In practice, we compute $W(s) = \langle[u(s) - u(0)]^2\rangle - \langle[u(s) - u(0)]\rangle^2$, where $\langle ...\rangle$ is the average when considering every vortex as the origin. u is the displacement of the i-th vortex located at $s_\parallel(s_\perp)$ from the i-th site of a perfect chain of vortices with lattice spacing $a_\parallel$ ($a_\perp$) averaged in a given row(lane).

For disordered elastic systems, the displacement correlator typically grows with distance with a roughness exponent 2ζ given by the universality-class of the system along the considered direction.[42] Figure 4 (c) shows the dependence of W with $s_\parallel$ averaged over tens of vortex rows and panel (d) shows the evolution with $s_\perp$ averaged along tens of vortex lanes. For the two studied compounds, the data are reasonably well fitted with an algebraic growth with exponent $2\zeta \approx 1$ in both directions, at odds with expectations for a hyperuniform system. The fits yield a multiplicative factor A roughly three and a half times larger for the $s_\perp$ than for the $s_\parallel$ direction. This is another proof that from experimental evidence vortex density fluctuations are anisotropic in media with planar defects.

Simulations of a structure of interacting elastic vortex lines in media with planar defects

Here we gain insight on the origin of the anisotropic vortex density fluctuations in media with planar defects by means of Langevin dynamics simulations of vortex lines in three dimensions with an applied field in the z-direction. We consider a media with randomly-spaced parallel planar defects oriented with their normal pointing along the $s_\perp$-axis in an orthogonal coordinate system $(s_\perp, s_\parallel, z)$. We model N_v vortices as elastic lines discretized in the z-direction, such that $\mathbf{r}_i(z) \equiv$

$(s_{\perp,i}(z), s_{\parallel,i}(z))$ describe the two-dimensional coordinate of vortex i at the layer $z = 1, ..., L_z$ with L_z the total number of layers. Periodic boundary conditions are taken in all directions in a system of size $L_\perp \times L_\parallel \times L_z$. The total energy per unit length of the structure of elastic lines is $E[\{\mathbf{r}_i(z)\}] = E_v + E_{vv} + E_{PD}$. Each line has an elastic tension energy given by Hook couplings of strength k

$$E_v[\{\mathbf{r}_i(z)\}] = \sum_{i=1}^{N_v}\sum_{z=1}^{L_z}\frac{k}{2}|\mathbf{r}_i(z+1) - \mathbf{r}_i(z)|^2, \qquad (1)$$

with $k = \epsilon_0/\lambda_{ab}^2$ a local harmonic approximation for the single vortex elastic tension, $\epsilon_0 \equiv \phi_0^2/(8\pi^2\lambda_{ab}^2)$ the interaction energy-scale per unit length, and λ_{ab} the in-plane penetration length. The repulsive interaction energy between three-dimensional vortex-lines derived from the London model[23] is

$$E_{vv}[\{\mathbf{r}_i(z)\}] = \sum_{i\neq j}^{N_v}\sum_{z=1}^{L_z}\epsilon_0 K_0\left(\frac{|\mathbf{r}_j(z) - \mathbf{r}_i(z)|}{\lambda_{ab}}\right), \qquad (2)$$

with $K_n(x)$ the nth-order modified Bessel function of the second kind. The pinning energy due to N_d defects is modeled as Gaussian-well channels

$$E_{PD}[\{\mathbf{r}_i(z)\}] = -A_{pin}\sum_{n=1}^{N_d}\sum_{i=1}^{N_v}\sum_{z=1}^{L_z} e^{-\frac{(s_{\perp,i}(z)-X_n)^2}{2\xi_{ab}^2}} \qquad (3)$$

where ξ_{ab} is the in-plane coherence length, A_{pin} the pinning strength of the planar defects, and X_n the random positions of the planar defects uniformly sampled along $L_\perp$. Finite-temperature Langevin dynamics simulations of the system are performed to obtain equilibrated low temperature configurations (see Methods). A snapshot of a configuration is shown in Fig.5 (a).

Figures 5 (a) and (b) show the main results of the simulations that are in accordance with experimental observations: i) The $S_\theta(q)$ is anisotropic and displays similar density fluctuations for all $\theta \neq 0$ directions; ii) fluctuations in the $q_\perp$ ($\theta = 0$) transverse direction are orders of magnitude larger, particularly at low q. The peak in the transverse direction is detected at a smaller wavenumber than in other directions, and $a_\perp > a_\parallel$ is also found in the simulations. Thus, this model of a structure of interacting elastic vortex lines nucleated in planar defects that are in controlled positions allow us to ascertain that the pinning generated by defects is strong enough as to increase the vortex density inside defects above the average. Furthermore, this model reveals that the anisotropic suppression of hyperuniformity has origin in the interactions allowing important vortex density fluctuations at large wavelengths for vortices caged in defects but also allowing for a rarefied distribution of vortices in between defects. As discussed in detail in the next section, by performing simulations and analytical calculations of a simplified version of the model of Eqs.(1),(2) and (3) we can go further in the comparison between experiments and theory, and show that the number of layers L_z (proportional to the sample thickness), plays a very relevant role in assessing hyperuniformity.

Discussion

The suppression of disordered hyperuniformity in media with planar defects can be discussed in a broader context than that of its implications for the synthesis of hyperuniform materials. This issue is connected to the related problem of the structural phases stabilized in media with different types of disorder. In the case of planar defects oriented in the direction of the magnetic flux as we study here, the stabilization of a robust planar-glass phase is expected.[43,44] In this phase, the positional correlation function is expected to decay exponentially,[43,44] implying both, a displacement correlator function $W \sim s_\perp$, and a structure factor behaving as $S_{\theta=0}(q \to 0) = \text{const} \neq 0$. These theoretical implications are consistent with our experimental and theoretical findings on the suppression of hyperuniformity in the direction transverse to planar defects. Nevertheless, these theoretical works do not study the vortex density fluctuations in the direction longitudinal to planar defects nor the experimentally relevant size-effects. The saturation at a finite value in the longitudinal direction $S_{\theta=90}(q \to 0)$, appreciably smaller than $S_{\theta=0}(q \to 0)$, is a subtle issue. Indeed, we argue below that at low densities, the vortex structure confined in a planar defect can be disordered hyperuniform provided the sample is thick enough and the confinement is strong.

In order to sustain these claims, we start by highlighting some relevant findings. First, both in experiments and simulations, the vortex structure in samples with planar defects presents well defined vortex rows. Simulations also show that at low temperatures most of vortex rows are parallel to planar defects. Second, the average vortex spacing along a row is appreciably smaller than in between rows, for instance $a_\parallel \sim 0.7a_\perp$ in the experiments. This indicates that intra-row vortex-vortex interactions are stronger than inter-row ones, motivating a single-row-based mean-field-like phenomenological approach.

Then, to further sustain our claims based in an analytical insight of the problem, we now consider a simplified model that captures the essential physical ingredients of the problem: We neglect the interaction between vortex rows as well as transverse vortex fluctuations, and model the system as a non-interacting collection of single vortex rows with strongly localized vortices inside a planar defect. We also neglect for the moment the effect of quenched point disorder since it is expected to be weaker than the planar defect pinning. The thermally-equilibrated configuration of the elastic system can then be obtained analytically in the elastic approximation by using the displacement field $u_1(s_\parallel, z)$. This field describes the mismatch of the planar vortex row with respect to a perfectly periodic chain of straight vortices aligned in the $s_\parallel$-direction, see Fig. 5(c). Within this simple model, as detailed in Methods, the large-wavelength density fluctuations at a single layer z give a structure factor

$$S_1(q_\parallel) \sim q_\parallel^2 \langle |\hat{u}_1(q_\parallel, z)|^2 \rangle \approx \begin{cases} \dfrac{n_0 k_B T}{\sqrt{c_{11} c_{44}}} q_\parallel & q_\parallel > \dfrac{2\pi}{l_{FS}} \\ \dfrac{n_0 k_B T}{c_{11} t} & q_\parallel < \dfrac{2\pi}{l_{FS}} \end{cases} \quad (4)$$

where $\hat{u}_1(q_\parallel, z)$ is the Fourier transform of the displacement field, c_{11} and c_{44} are the compression and tilt elastic modulii of the planar vortex system, t is the sample thickness, and l_{FS} is a relevant crossover length. Assuming translation symmetry along z, Eq.(4) implies that in real space the displacement correlator in the longitudinal direction to planar defects scales as

$$W(s_\parallel) \sim \begin{cases} \log(s_\parallel) & s_\parallel < l_{FS} \\ s_\parallel & s_\parallel > l_{FS}, \end{cases} \quad (5)$$

see Methods for further details. The result of a $\log(s_\parallel)$ roughness is not a surprise since the system is essentially a thermally-fluctuating two-dimensional elastic lattice. The novelty here is that to explain the experimental observations it is necessary to consider the finite-thickness induced crossover distance

$$l_{FS} \approx \frac{t}{2\pi} \sqrt{\frac{c_{11}}{c_{44}}} \ . \quad (6)$$

This crossover behaviour in $S_1(q_\parallel)$ and $W(s_\parallel)$ is also confirmed in numerical simulations of a single vortex row confined in a planar defect for different thicknesses, see Fig.5 (d). Furthermore, the top-left insert of this figure shows that all $S_1(q_\parallel)t$ vs. $q_\parallel t$ curves collapse into a master-curve, confirming quantitatively that $l_{FS} \propto t$, Eq.(6). According to Eq. (4), in the thermodynamic limit $l_{FS} \to \infty$, and the vortex row at a constant-z cross section is class II hyperuniform since $S_1(q_\parallel) \sim q_\parallel^\alpha$ with $\alpha = 1$.[2] This hyperuniformity class contrasts with more ordered class I hyperuniform systems where $\alpha > 1$.[2] However, in systems with finite thickness, Eq.(4) predicts a crossover towards a non-hyperuniform behaviour for $s_\parallel > l_{FS}$. This corresponds to a dimensional crossover from a two-dimensional to an effective one-dimensional elastic system equivalent to an elastic chain composed by rigid vortices. Interestingly, this phenomenology is closely related to the crossover predicted for Luttinger liquids at a characteristic thermal length.[45]

A caveat in our model might be that we ignore that real samples have weak point disorder. However, as shown in Methods, if this disorder is considered, the main results of Eqs.(4), (5) and (6) remain qualitatively valid. Namely, for $s_\parallel > l_{FS}$ $S_1(q_\parallel \to 0) = \text{const}$ and $W(s_\parallel \to \infty) \sim s_\parallel$ while for $s_\parallel < l_{FS}$, the structure is disordered hyperuniform but class III ($\alpha < 1$) instead of class II ($\alpha = 1$).[2]

Finally, we argue that a finite size effect is a plausible explanation for the suppression of hyperuniformity observed in experiments and simulations. Considering the vortex-vortex interaction potential per unit length $U(x) \approx \epsilon_0 K_0(x/\lambda)$, with $\epsilon_l \sim \epsilon_0$ the single vortex elastic tension, the elastic constants of the planar vortex system can be estimated as $c_{11} \approx aU''(a)$ and $c_{44} \approx \epsilon_l/a$.[46] Thus, using these approximations in Eq.6, the crossover length can be estimated by considering only the sample thickness since we get $l_{FS} \approx (t/2\pi)(a/\lambda)\sqrt{(K_0(a/\lambda) + K_2(a/\lambda))/2}$. Provided $a \sim 3\lambda$ in the experiments, l_{FS} shortens with either decreasing t or $1/a$. In the studied samples with $t \sim 5 - 30\,\mu$m,[41] $l_{FS} \approx t/10 \sim a$, and then this dimensional crossover is quite likely at the origin of the observation of a non-vanishing structure factor for large wavelengths. For thick enough samples and/or smaller a such that $l_{FS} \gtrsim 10\,a$, the crossover to disordered hyperuniform vortex density fluctuations might be observed experimentally. This would be a state with directional hyperuniformity.[47] In other words, vortex matter nucleated in thin samples with a dense distribution of planar defects effectively behave as a collection of one-dimensional elastic manifolds. The suppression of hyperuniformity in elastic structures nucleated in media with planar disorder as identified in this work may be also observed in a broad spectrum of systems with a control parameter tuning the dimensional crossover. In addition, a direct mapping between the thickness of a classical system and the temperature in quantum systems can be made, signposting the conditions for disordered hyperuniformity to persist in planarly-confined quantum systems such as optical traps. These results are rather important on the search for novel disordered hyperuniform classic and quantum materials presenting exotic physical properties.

I. METHODS

Sample preparation and characterization

We studied $Bi_2Sr_2CaCu_2O_{8+\delta}$ and $YBa_2Cu_3O_7$ samples grown and characterized by means of X-ray diffraction, transport and magnetometry techniques. The $Bi_2Sr_2CaCu_2O_{8+\delta}$ samples with point disorder and few planar defects were grown by means of the flux method and have a $T_c \sim 90$ K; further details on the crystallographic and superconducting properties of these samples can be found in Ref. 48. The $Bi_2Sr_2CaCu_2O_{8+\delta}$ samples with many planar defects were grown following the travelling-solvent-floating-zone method using an image furnace with two ellipsoidal mirrors and has a critical temperature of ~ 87 K. The $YBa_2Cu_3O_7$ single crystals were obtained following a growth from the melt technique and are fully oxygenated with $T_c \sim 92$ K, see Ref. 49 for further details on the growing method.

Vortex imaging by means of magnetic decoration experiments

We image individual vortex positions at the sample surface in large fields-of-view ranging from 1,000 to 35,000 vortices by means of magnetic decoration experiments.[50] For all the data presented here, the magnetic field is applied above T_c and the sample is cooled down to 4.2 K. At this temperature Fe particles are evaporated in a pressure-controlled helium chamber and clusters of these particles land on the sample surface decorating the positions of vortices. Even though the snapshots of the structure are taken at 4.2 K, during the field-cooling process the vortex structure gets frozen, at length-scales of the lattice parameter a_0, at a temperature $T_{\rm freez} \sim T_{\rm irr}$, the irreversibility temperature at which pinning (sample disorder) sets in.[51] On further cooling down to 4.2 K, vortices can move but in length scales of the order of coherence length, 200 times smaller than the typical size of a vortex as detected by magnetic decoration. Therefore the structure imaged by magnetic decoration at 4.2 K corresponds to the equilibrium one at $T_{\rm freez}$.

Structure factors

In order to calculate the structure factors we start considering the vortex density modulation

$$\rho(x,y,z) = \frac{1}{t}\Sigma_{j=1}^{N_{\rm v}}\delta(x-x_j(z))\delta(y-y_j(z)) - \rho_0. \quad (7)$$

where ρ_0 is the average density and $N_{\rm v}$ the number of vortices. In magnetic decoration experiments we have access to the vortex structure at the surface, namely $\rho(x,y,z=0)$. The structure factor is obtained from the two-dimensional Fourier transform of the density, $\hat{\rho}$, as

$$S(\mathbf{q}) = |\hat{\rho}(q_x,q_y,z=0)|^2. \quad (8)$$

In the same token, the one-dimensional structure factor in a vortex row, S_1 is obtained from the vortex density modulation along a line $\hat{\rho_1}$. The angular structure factor $S_\theta(q)$ is the polar-coordinate representation of $S(q_x,q_y)$, see Fig. 2 (f) for schematics.

The angularly-averaged $\langle S(q)\rangle$ has to be calculated carefully when studying the low-q density modes. Due to finite size effects, the borders and shape of the experimental field-of-view hinder the study of $S(\mathbf{q})$ in the low-q range due to the annoying windowing effect. In rectangular fields-of-view as we study here, this artifact produces an excess in $S(q_{\rm x},q_{\rm y})$ in a cross-shaped region centered at $q_{\rm x}=q_{\rm y}=0$. When analyzing our experimental data, in order to get rid of this effect we neglect the contribution from this cross. In simulations, this effect is avoided considering in-plane periodic boundary conditions.

Computer simulation details

The numerical simulations performed here consider an overdamped Langevin dynamics at a temperature T

$$\eta\ \ \partial_\tau \mathbf{r}_i(z) = -\frac{\delta E}{\delta \mathbf{r}_i(z)} + \xi(\mathbf{r}_i(z),\tau) \quad (9)$$

$$\langle\ \ \xi(\mathbf{r}_i,\tau)\xi(\mathbf{r}'_j,\tau')\rangle = 2\eta k_{\rm B}T\delta_{ij}\delta(\tau-\tau') \quad (10)$$

where τ is the time and η is the Bardeen-Stephen friction. In order to emulate the experimental conditions we have simulated systems with densities such that $a = 3\lambda_{\rm ab}$. The values of the pinning strength of planar defects, $A_{\rm pin}$, and the number of planar defects, $N_{\rm d}$, were tuned such that the vortex system displays at the surface of the simulated sample a structure qualitatively similar to the one observed in magnetic decoration experiments. We have used $L_{\rm z}=64$, $N_{\rm v}=40$ and $a_0=3\lambda_{\rm ab}$, $A_{\rm pin}=0.2\epsilon_0$, $k=\epsilon_0/\lambda_{\rm ab}^2$, $N_{\rm d}=38$, $L_\parallel = 60\lambda_{\rm ab}$, $L_\perp = L_\parallel\sqrt{3}/2$. In order to mimic the experiments we start the simulation at $T=0.5\epsilon_0\lambda_{\rm ab}/k_{\rm B}$, reduce T slowly, and equilibrate the system at $T=0.001\epsilon_0/k_{\rm B}$. When the averaged structure factor appears to be stationary, we analyze different properties of the final configuration and average them over several realizations of the same protocol.

Planar elastic vortex array model: Analytical details

The simple model of a planar elastic vortex array considered in the discussion is described in the continuum by the scalar longitudinal displacement field $u_1(s_\parallel,z)$ with hamiltonian

$$\mathcal{H} \approx \int dq_{\rm z}dq_\parallel |\hat{u}_1(q_\parallel,q_{\rm z})|^2[c_{11}(q_\parallel,q_{\rm z})q_x^2 + c_{44}(q_\parallel,q_{\rm z})q_{\rm z}^2], \quad (11)$$

where $\hat{u}_1(q_\parallel,q_{\rm z})$ is the Fourier transform of $u_1(s_\parallel,z)$ and $c_{11}(q_\parallel,q_{\rm z})$ and $c_{44}(q_\parallel,q_{\rm z})$ are the dispersive compression and tilt elastic modulii. At thermal equilibrium

$$\langle|\hat{u}_1(q_\parallel,q_{\rm z})|^2\rangle = \frac{k_{\rm B}T}{c_{11}(q_\parallel,q_{\rm z})q_\parallel^2 + c_{44}(q_\parallel,q_{\rm z})q_{\rm z}^2}. \quad (12)$$

The modulation of the coarse-grained vortex density at long-wavelengths is

$$\delta n(s_\parallel,z) \approx -n_0\partial_{s_\parallel}u_1(s_\parallel,z), \quad (13)$$

where n_0 is the average number of vortices per unit length along the vortex row of the planar vortex array. Then, for small $q_\parallel$,

$$n_0 S_1(q_\parallel,q_{\rm z}) \equiv \langle|\delta\hat{n}(q_\parallel,q_{\rm z})|^2\rangle \approx n_0 q_\parallel^2\langle|\hat{u}_1(q_\parallel,q_{\rm z})|^2\rangle. \quad (14)$$

By assuming translational invariance along z and evaluating the elastic constants at $q_z = 2\pi/t$, the correlation function

$$\begin{aligned} S_1(q_\parallel, z_1-z_2) &= n_0^{-1}\langle\delta\hat{n}(q_\parallel,z_1)\delta\hat{n}^*(q_\parallel,z_2)\rangle \\ &\approx \frac{n_0 k_{\rm B}T e^{-|z_1-z_2|/\xi_\parallel(q_\parallel)}}{c_{11}(q_\parallel,2\pi/t)\xi_\parallel(q_\parallel)}, \end{aligned} \quad (15)$$

with

$$\xi_{\parallel}(q_{\parallel}) = q_{\parallel}^{-1}\sqrt{c_{44}(q_{\parallel}, 2\pi/t)/c_{11}(q_{\parallel}, 2\pi/t)} \quad (16)$$

the correlation length along the z-direction. Neglecting surface effects,[52] the structure factor at the sample surface is $S_1(q_{\parallel}) \equiv S_1(q_{\parallel}, z_1 - z_2 = 0)$. Then, for $\xi_{\parallel}(q_{\parallel}) < t$ we get Eq. (4). Finite-size effects appear when $\xi_{\parallel}(2\pi/l_{\rm FS}) = t$, obtaining the crossover length l_{FS} of Eq.(6).

When weak point disorder is added, the dimensional crossover still exists and the effective rigid-vortex chain regime for $q_{\parallel} < 2\pi/l_{\rm FS}$ is equivalent to an elastic interface in a random-periodic type of disorder. In this case, at equilibrium[53]

$$\langle|\hat{u}_1(q_{\parallel})|^2\rangle \sim q_{\parallel}^{-(1+2\zeta_{\parallel})} \quad (17)$$

with $\zeta_{\parallel} = 1/2$. Since $S_1(q_{\parallel}) = q_{\parallel}^2\langle|\hat{u}_1(q_{\parallel})|^2\rangle$, the second regime of Eqs. (4) and (5) is obtained for $q_{\parallel} < 2\pi/l_{\rm FS}$ or $s_{\parallel} > l_{\rm FS}$. The correlations in the infinite-thickness limit can be tackled analytically by mapping to the Cardy-Ostlund model.[46] In this case W displays subtle additive $\log^2(s_{\parallel})$ corrections to the $\log(s_{\parallel})$ growth, [46] implying

$$S_1(q_{\parallel} \to 0) \sim -q_{\parallel}\log(q_{\parallel}) \to 0. \quad (18)$$

Then, in this limit the system is class III hyperuniform in contrast with the class II hyperuniformity found in the clean case.

Once the corresponding formulas for $S_1(q_{\parallel})$ are known, the displacement correlator of Eq. (5) of the main text can be obtained considering that

$$\begin{aligned} W &= \langle[u_1(s_{\parallel}, z) - u_1(0, z)]^2\rangle - \langle[u_1(s_{\parallel}, z) - u_1(0, z)]\rangle^2 \\ &\sim \int dq_{\parallel}\ q_{\parallel}^{-2}S_1(q_{\parallel})(1 - \cos(q_{\parallel}s_{\parallel})). \end{aligned} \quad (19)$$

Data availability

All relevant data are available from the authors upon request.

Code availability

All relevant code for simulations are available from the authors upon request.

References

[1] S. Torquato and F. H. Stillinger, Phys. Rev. E **68**, 041113 (2003), URL https://link.aps.org/doi/10.1103/PhysRevE.68.041113.

[2] S. Torquato, Phys. Rep. **745**, 1 (2018), ISSN 0370-1573, URL https://www.sciencedirect.com/science/article/pii/S037015731830036X.

[3] W. Man, M. Florescu, E. P. Williamson, Y. He, S. R. Hashemizad, B. Y. C. Leung, D. R. Liner, S. Torquato, P. M. Chaikin, and P. J. Steinhardt, Proc. Natl. Acad. Sci. USA **110**, 15886 (2013), ISSN 0027-8424, URL https://www.pnas.org/content/110/40/15886.

[4] D. Chen and S. Torquato, Acta Materialia **142**, 152 (2018), ISSN 1359-6454, URL https://www.sciencedirect.com/science/article/pii/S1359645417308194.

[5] Y. Zheng, L. Liu, H. Nan, Z.-X. Shen, G. Zhang, D. Chen, L. He, W. Xu, M. Chen, Y. Jiao, et al., Sci. Adv. **6**, eaba0826 (2020).

[6] M. Salvalaglio, M. Bouabdellaoui, M. Bollani, A. Benali, L. Favre, J.-B. Claude, J. Wenger, P. de Anna, F. Intonti, A. Voigt, et al., Phys. Rev. Lett. **125**, 126101 (2020), URL https://link.aps.org/doi/10.1103/PhysRevLett.125.126101.

[7] D. Chen, Y. Zheng, C.-H. Lee, S. Kang, W. Zhu, H. Zhuang, P. Y. Huang, and Y. Jiao, Phys. Rev. B **103**, 224102 (2021), URL https://link.aps.org/doi/10.1103/PhysRevB.103.224102.

[8] D. Chen, Y. Zheng, L. Liu, G. Zhang, M. Chen, Y. Jiao, and H. Zhuang, Proc. Natl. Acad. Sci. USA **118**, e2016862118 (2021), ISSN 0027-8424, URL https://www.pnas.org/content/118/3/e2016862118.

[9] C. E. Zachary, Y. Jiao, and S. Torquato, Phys. Rev. Lett. **106**, 178001 (2011), URL https://link.aps.org/doi/10.1103/PhysRevLett.106.178001.

[10] R. Dreyfus, Y. Xu, T. Still, L. A. Hough, A. G. Yodh, and S. Torquato, Phys. Rev. E **91**, 012302 (2015), URL https://link.aps.org/doi/10.1103/PhysRevE.91.012302.

[11] A. T. Chieco and D. J. Durian, Phys. Rev. E **103**, 062609 (2021), URL https://link.aps.org/doi/10.1103/PhysRevE.103.062609.

[12] G. Rumi, J. Aragón Sánchez, F. Elías, R. Cortés Maldonado, J. Puig, N. R. Cejas Bolecek, G. Nieva, M. Konczykowski, Y. Fasano, and A. B. Kolton, Phys. Rev. Res. **1**, 033057 (2019), URL https://link.aps.org/doi/10.1103/PhysRevResearch.1.033057.

[13] J. B. Llorens, I. Guillamón, I. G. Serrano, R. Córdoba, J. Sesé, J. M. De Teresa, M. R. Ibarra, S. Vieira, M. Ortuño, and H. Suderow, Phys. Rev. Res. **2**, 033133 (2020), URL https://link.aps.org/doi/10.1103/PhysRevResearch.2.033133.

[14] Y. Jiao, T. Lau, H. Hatzikirou, M. Meyer-Hermann, J. C. Corbo, and S. Torquato, Phys. Rev. E **89**, 022721 (2014), URL https://link.aps.org/doi/10.1103/PhysRevE.89.022721.

[15] Y. Zheng, Y.-W. Li, and M. P. Ciamarra, Soft Matter **16**, 5942 (2020), URL http://dx.doi.org/10.1039/D0SM00776E.

[16] A. Gabrielli, B. Jancovici, M. Joyce, J. L. Lebowitz, L. Pietronero, and F. Sylos Labini, Phys. Rev. D **67**, 043506 (2003), URL https://link.aps.org/doi/10.1103/PhysRevD.67.043506.

[17] M. A. Klatt, J. Lovrić, D. Chen, S. C. Kapfer, F. M. Schaller, P. W. A. Schönhöfer, B. S. Gardiner, A.-S. Smith, G. E. Schröder-Turk, and S. Torquato, Nature Comm. **10**, 811 (2019), ISSN 2041-1723, URL https://doi.org/10.1038/s41467-019-08360-5.

[18] M. Florescu, S. Torquato, and P. J. Steinhardt, Proc. Nat. Acad. Sci. USA **106**, 20658 (2009).

[19] L. S. Froufe-Pérez, M. Engel, P. F. Damasceno, N. Muller, J. Haberko, S. C. Glotzer, and F. Scheffold, Phys. Rev. Lett. **117**, 053902 (2016), URL https://link.aps.org/doi/10.1103/PhysRevLett.117.053902.

[20] Q. Le Thien, D. McDermott, C. J. O. Reichhardt, and C. Reichhardt, Phys. Rev. B **96**, 094516 (2017), URL https://link.aps.org/doi/10.1103/PhysRevB.96.094516.

[21] I. A. Sadovskyy, A. E. Koshelev, W.-K. Kwok, U. Welp, and A. Glatz, Proc. Nat. Acad. Sci. USA **116**, 10291 (2019), ISSN 0027-8424, URL https://www.pnas.org/content/116/21/10291.

[22] R. Cubitt, E. M. Forgan, G. Yang, S. L. Lee, D. M. Paul, H. A. Mook, M. Yethiraj, P. H. Kes, T. W. Li, A. A. Menovsky, et al., Nature **365**, 407 (1993), ISSN 1476-4687, URL https://doi.org/10.1038/365407a0.

[23] G. Blatter, M. V. Feigel'man, V. B. Geshkenbein, A. I. Larkin, and V. M. Vinokur, Rev. Mod. Phys. **66**, 1125 (1994), URL https://link.aps.org/doi/10.1103/RevModPhys.66.1125.

[24] F. Pardo, F. de la Cruz, P. L. Gammel, E. Bucher, and D. J. Bishop, Nature **396**, 348 (1998), ISSN 1476-4687, URL https://doi.org/10.1038/24581.

[25] T. Klein, I. Joumard, S. Blanchard, J. Marcus, R. Cubitt, T. Giamarchi, and P. Le Doussal, Nature **413**, 404 (2001), ISSN 1476-4687, URL https://doi.org/10.1038/35096534.

[26] M. Menghini, Y. Fasano, and F. de la Cruz, Phys. Rev. B **65**, 064510 (2002), URL https://link.aps.org/doi/10.1103/PhysRevB.65.064510.

[27] A. Pautrat, C. Simon, C. Goupil, P. Mathieu, A. Brûlet, C. D. Dewhurst, and A. I. Rykov, Phys. Rev. B **75**, 224512 (2007), URL https://link.aps.org/doi/10.1103/PhysRevB.75.224512.

[28] A. P. Petrović, Y. Fasano, R. Lortz, C. Senatore, A. Demuer, A. B. Antunes, A. Paré, D. Salloum, P. Gougeon, M. Potel, et al., Phys. Rev. Lett. **103**, 257001 (2009), URL https://link.aps.org/doi/10.1103/PhysRevLett.103.257001.

[29] H. Suderow, I. Guillamón, J. G. Rodrigo, and S. Vieira, Supercond. Sci. Technol. **27**, 063001 (2014).

[30] M. Marziali Bermúdez, M. R. Eskildsen, M. Bartkowiak, G. Nagy, V. Bekeris, and G. Pasquini, Phys. Rev. Lett. **115**, 067001 (2015), URL https://link.aps.org/doi/10.1103/PhysRevLett.115.067001.

[31] M. Zehetmayer, Scientific Reports **5**, 9244 (2015), ISSN 2045-2322, URL https://doi.org/10.1038/srep09244.

[32] S. Chandra Ganguli, H. Singh, G. Saraswat, R. Ganguly, V. Bagwe, P. Shirage, A. Thamizhavel, and P. Raychaudhuri, Scientific Reports **5**, 10613 (2015), ISSN 2045-2322, URL https://doi.org/10.1038/srep10613.

[33] R. Toft-Petersen, A. B. Abrahamsen, S. Balog, L. Porcar, and M. Laver, Nature Communications **9**, 901 (2018), ISSN 2041-1723, URL https://doi.org/10.1038/s41467-018-03267-z.

[34] J. Aragón Sánchez, R. Cortés Maldonado, N. R. Cejas Bolecek, G. Rumi, P. Pedrazzini, M. I. Dolz, G. Nieva, C. J. van der Beek, M. Konczykowski, C. D. Dewhurst, et al., Comm. Phys. Nat. **2**, 143 (2019).

[35] J. B. Llorens, L. Embon, A. Correa, J. D. González, E. Herrera, I. Guillamón, R. F. Luccas, J. Azpeitia, F. J. Mompeán, M. García-Hernández, et al., Phys. Rev. Res. **2**, 013329 (2020), URL https://link.aps.org/doi/10.1103/PhysRevResearch.2.013329.

[36] Y. Fasano and M. Menghini, Supercond. Sci. Tech. **21** (2008).

[37] M. R. Koblischka, R. J. Wijngaarden, D. G. de Groot, R. Griessen, A. A. Menovsky, and T. W. Li, Phys. C **249**, 339 (1995).

[38] J. Herbsommer, V. Correa, G. Nieva, H. Pastoriza, and J. Luzuriaga, Solid State Comm. **120**, 59 (2001), ISSN 0038-1098, URL https://www.sciencedirect.com/science/article/pii/S0038109801003490.

[39] I. Maggio-Aprile, C. Renner, A. Erb, E. Walker, and Ø. Fischer, Nature **390**, 487 (1997).

[40] Y. Fasano, J. Herbsommer, and F. de la Cruz, Phys. Stat. Sol. (b) **215**, 563 (1999).

[41] Y. Fasano, M. De Seta, M. Menghini, H. Pastoriza, and F. De la Cruz, Solid State Communications **128**, 51 (2003), URL https://doi.org/10.1016/S0038-1098(03)00645-8.

[42] A. L. Barabasi, H. E. Stanley, and L. M. Sander, Phys. Today **48**, 68 (1995), ISSN 1945-0699, URL http://dx.doi.org/10.1063/1.2808215.

[43] T. Emig and T. Nattermann, Phys. Rev. Lett. **97**, 177002 (2006), URL https://link.aps.org/doi/10.1103/PhysRevLett.97.177002.

[44] A. Petković, T. Emig, and T. Nattermann, Phys. Rev. B **79**, 224512 (2009), URL https://link.aps.org/doi/10.1103/PhysRevB.79.224512.

[45] T. Giamarchi, *Quantum physics in one dimension*, International series of monographs on Physics (Clarendon Press, Oxford, 2004), URL https://cds.cern.ch/record/743140.

[46] T. Nattermann and S. Scheidl, Adv. in Phys. **49**, 607 (2000).

[47] S. Torquato, Phys. Rev. E **94**, 022122 (2016), URL https://link.aps.org/doi/10.1103/PhysRevE.94.022122.

[48] V. F. Correa, E. E. Kaul, and G. Nieva, Phys. Rev. B **63**, 172505 (2001), URL https://link.aps.org/doi/10.1103/PhysRevB.63.172505.

[49] F. de la Cruz, D. López, and G. Nieva, Philos. Mag. B **70**, 773 (1994).

[50] Y. Fasano, M. De Seta, M. Menghini, H. Pastoriza, and F. de la Cruz, Proc. Nat. Acad. Sci. USA **102**, 3898 (2005), ISSN 0027-8424, URL https://www.pnas.org/content/102/11/3898.

[51] N. R. C. Bolecek, A. B. Kolton, M. Konczykowski, H. Pastoriza, D. Domínguez, and Y. Fasano, Phys. Rev. B **93**, 054505 (2016), URL https://link.aps.org/doi/10.1103/PhysRevB.93.054505.

[52] M. C. Marchetti and D. R. Nelson, Phys. Rev. B **47**, 12214 (1993), URL https://link.aps.org/doi/10.1103/PhysRevB.47.12214.

[53] S. Bustingorry, A. B. Kolton, and T. Giamarchi, Phys. Rev. B **82**, 094202 (2010), URL https://link.aps.org/doi/10.1103/PhysRevB.82.094202.

Acknowledgements

We thank Thierry Giamarchi for stimulating discussions.

This work was supported by the Argentinean National Science Foundation (ANPCyT) under Grants PICT 2017-2182 and PICT 2018-1533; by the Universidad Nacional de Cuyo research grants 06/C566 and 06/C575; and by Graduate Research fellowships from CONICET for J. R. P., F. E., J. A. S., R. C. M., G. R. and N. R. C. B.

Author contributions

Y.F. and A.B.K. designed research and discussed the general method to analyze the data, Y. F. and R.C.M. performed measurements, G.N. and P. P. grew samples, F. E. and A. B. K. performed simulations and theoretical calculations, J. R. P., F. E., J.A.S., G. R., A. B. K. and Y.F. analyzed data; all authors discussed the data analysis and interpretation; Y.F. and A.B.K. wrote the paper.

Competing interests

The authors declare no competing interests.

Additional information

Correspondence and requests for materials should be addressed to Y.F.

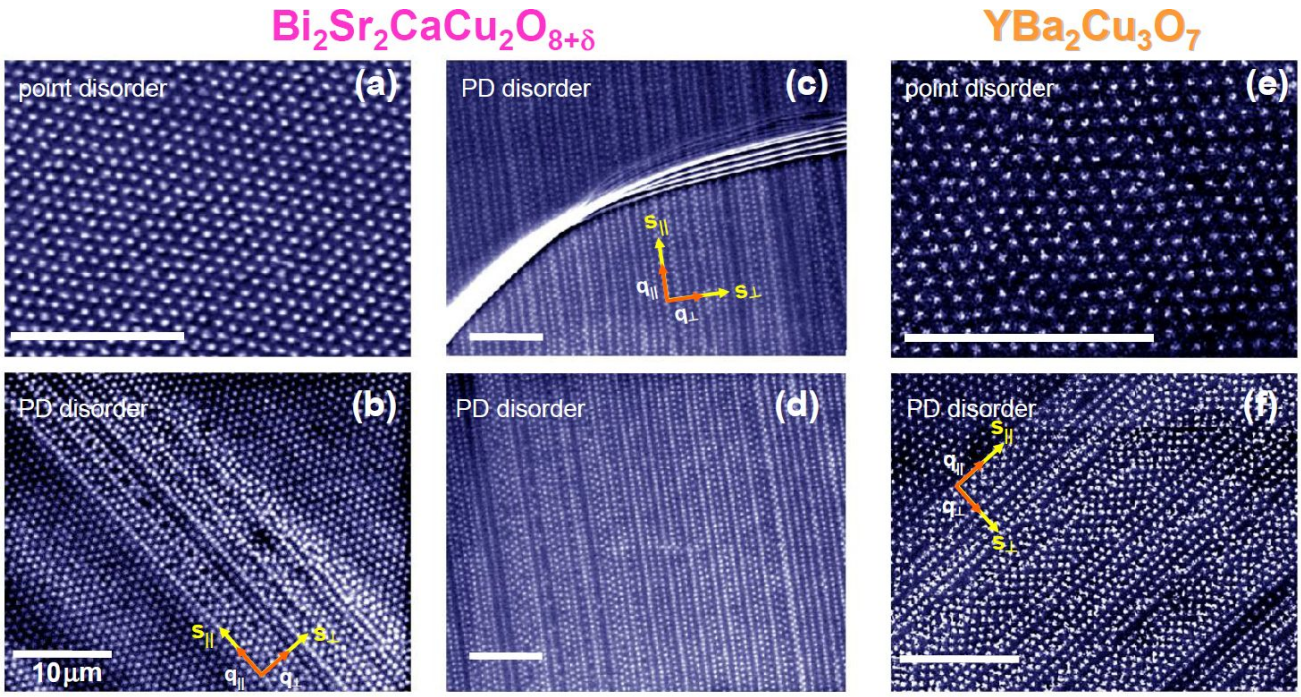


Figure 1: **Magnetic decoration imaging of vortices in samples with point and planar defects.** Vortices (white dots) nucleated at 30 G in $Bi_2Sr_2CaCu_2O_{8+\delta}$ (a-d) and $YBa_2Cu_3O_7$ (e-f) samples with point (a,e) and planar (b,c,d,f) disorder. Vortices nucleated on planar defects are seen as *vortex rows* with a density in general larger than the average. Results in $Bi_2Sr_2CaCu_2O_{8+\delta}$ samples presenting few (b) and many (c,d) planar defects in millimeter-sized crystals. (c) Illustration on how the planar defects extend on the bulk of the sample: The vortex rows continue in the same in-plane direction in the vicinity of a micron-height step generated by cleaving. The $s_\parallel$-$s_\perp$ coordinate system oriented along and perpendicular to the planar defects (PD), and the corresponding wave vectors $q_\parallel$ and $q_\perp$, are shown in some images. White scale bars correspond to 10 μm and labels indicating the dominant disorder are shown in each case.

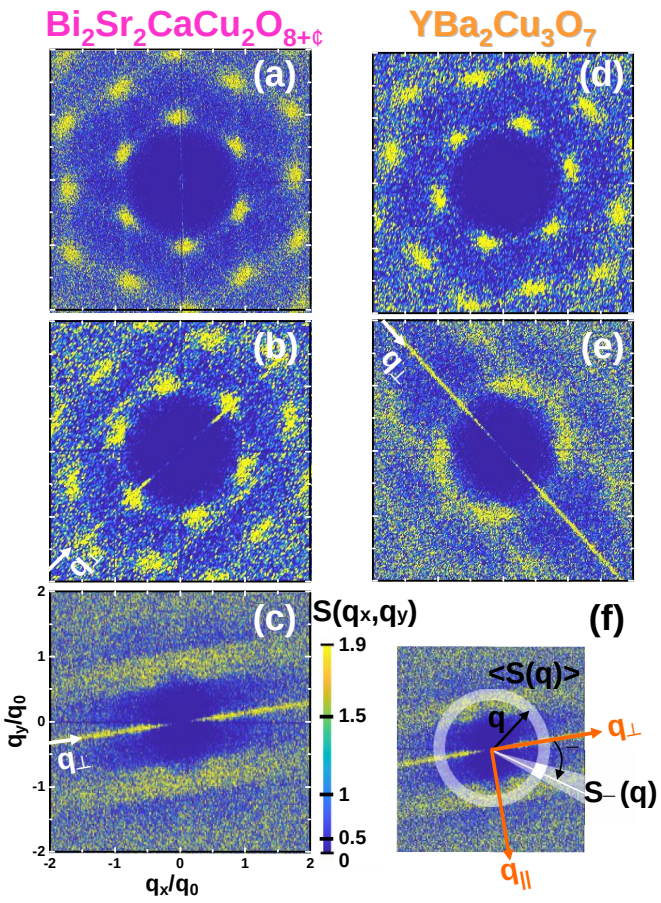


Figure 2: **Structure factor of vortices nucleated in type-II superconducting samples with point and planar disorder.** Data in $Bi_2Sr_2CaCu_2O_{8+\delta}$ samples with (a) point disorder, (b) few and (c) many planar defects (9,200, 2,000 and 35,000 vortices). Data in $YBa_2Cu_3O_7$ samples with (d) point disorder and (e) many twin boundaries (2,300 and 4,000 vortices). The color-scale is cuadratic (see bar) and wavenumbers are normalized by the Bragg wavenumber $q_0 = 2\pi/a$ with a the average distance between first-neighbor vortices. (f) Schematics of the computation of the angularly-averaged $\langle S(q)\rangle$ and angular $S_\theta(q)$ structure factors: Pixels considered to obtain these magnitudes are highlighted as a donut and an angular section, respectively. Shown are the wave-vector q, angle θ, and the reciprocal-space directions $q_\parallel$ and $q_\perp$.

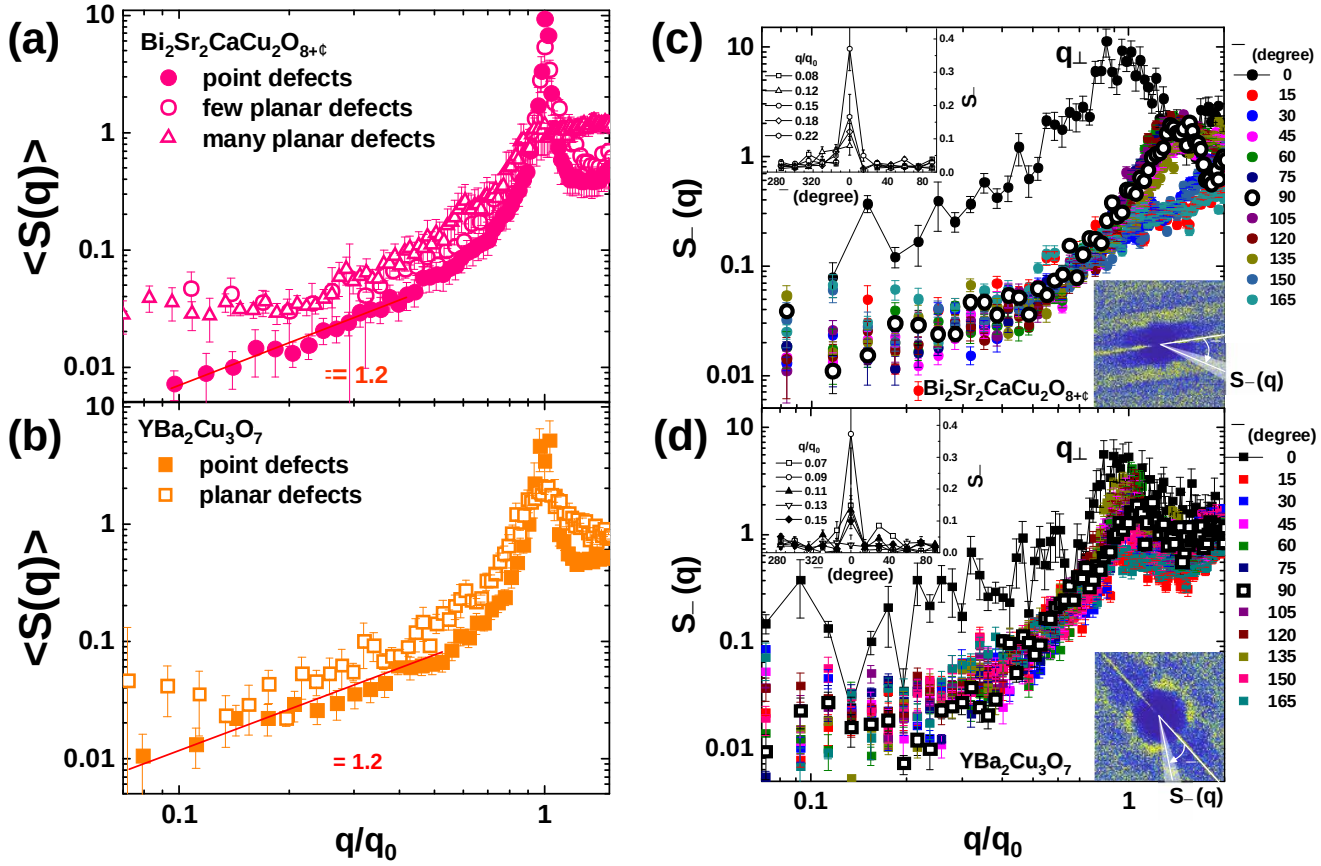


Figure 3: **Evidence supporting the suppression of hyperuniformity in media with planar defects.** Angularly-averaged structure factor of the vortex structures nucleated in (a) $Bi_2Sr_2CaCu_2O_{8+\delta}$ and (b) $YBa_2Cu_3O_7$ samples with point (full symbols) and planar (open symbols) defects. The wavenumber is normalized by the Bragg wavenumber $q_0 = 2\pi/a$. Full red lines are fits to the data in samples with point disorder considering $\langle S(q)\rangle \sim (q/q_0)^\beta$ when $q/q_0 \to 0$ yielding $\beta = 1.2 \pm 0.2$. Angular $S_\theta(q)$ structure factor of vortex matter nucleated in (c) $Bi_2Sr_2CaCu_2O_{8+\delta}$ and (d) $YBa_2Cu_3O_7$ samples with planar defects. Curves obtained averaging the $S(q_x, q_y)$ data shown in the inserts considering $\pm\delta\theta = 7.5$ degree around the azimuthal angles θ indicated in the legends. Black points correspond to $S_{\theta=0}(q)$ in the transversal direction $q_\perp$; white-with-black-edge points show $S_{\theta=90}(q)$ in the longitudinal $q_\parallel$ direction; color points correspond to intermediate directions. In the $q \to 0$ limit all curves tend to saturate, but the color and white points form a bunch of data saturating at a smaller value than data for the transversal direction. Left-top inserts: S_θ as a function of θ for fixed values of q/q_0 (vertical cuts of data shown in the main panels). Error bars represent the standard deviation of data when averaging at a given q.

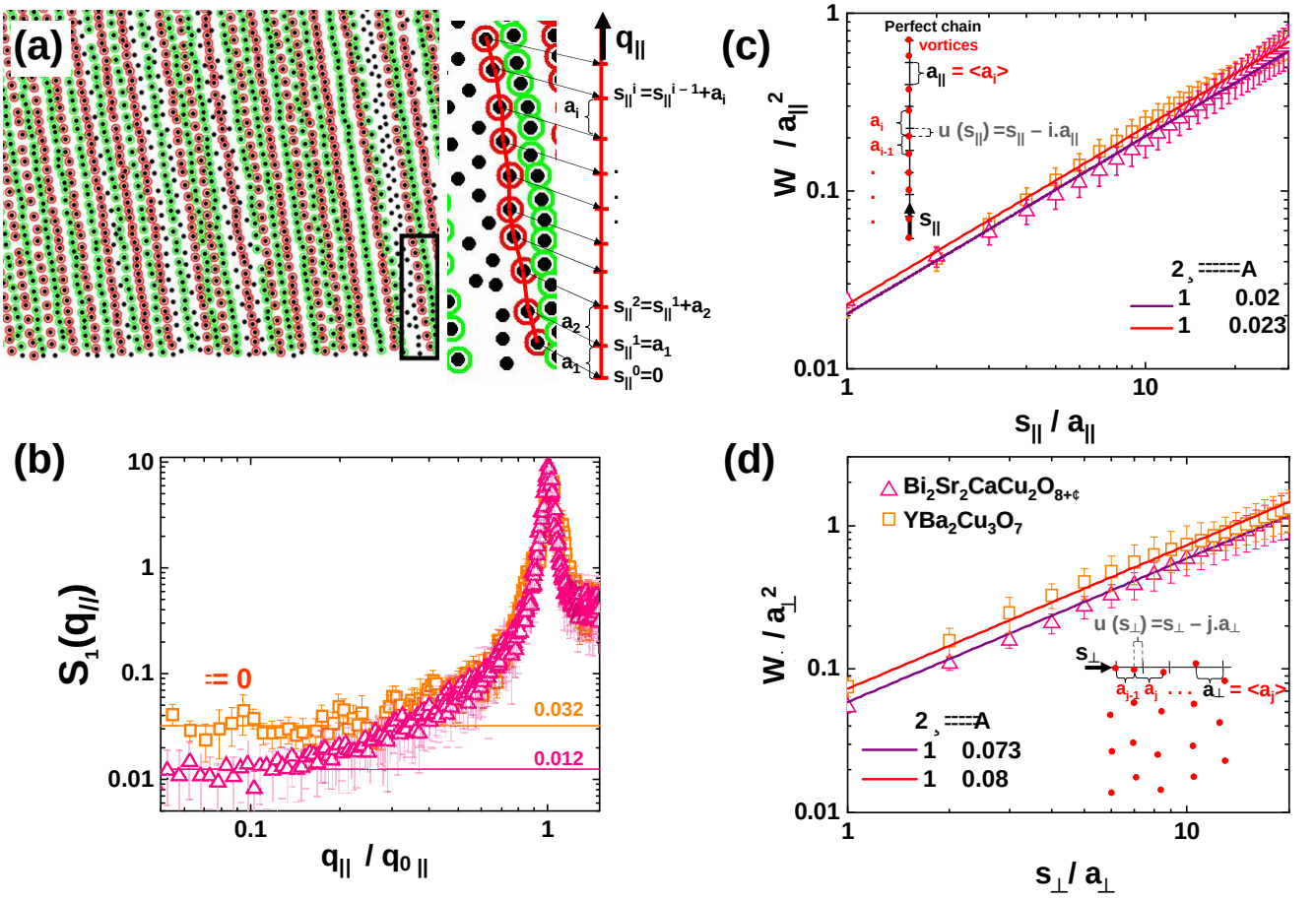


Figure 4: **Anisotropy in the large-scale vortex density fluctuations in samples with planar defects.** (a) Left: Detail of the digitalized vortex positions (black dots) in a region of the $Bi_2Sr_2CaCu_2O_{8+\delta}$ sample with many planar defects. Vortices highlighted in red or green belong to the same vortex row; non-highlighted vortices are presumably interstitial to the vortex rows. Right: Zoom-in of the structure in the black-framed region. In a given row, vortices are labeled and a_i is the distance between vortices i and $i+1$. Then the vortex row is mapped in a straight line where adjacent vortices are spaced in a_i and the coordinate of vortex $i+1$ is $s_{\parallel}^{i}$. (b) After performing this mapping of vortex positions in a straight line, the average one-dimensional structure factor along the direction of defects, $S_1(q_\parallel)$ is computed (see text for details) averaging data coming from $\sim$ 50 (12) rows containing 9,000 (1,300) vortices in $Bi_2Sr_2CaCu_2O_{8+\delta}$ ($YBa_2Cu_3O_7$). Fits considering an algebraic decay of $S_1(q_\parallel)$ for $q_\parallel \to 0$ yield $\beta = 0$ within the error, for both materials. (c) Displacement correlator $W/a_\parallel^2$ calculated along the $s_\parallel$ direction of vortex rows (statistics for 1,500 vortices in $Bi_2Sr_2CaCu_2O_{8+\delta}$ and 1,300 in $YBa_2Cu_3O_7$). Insert: Schematic representation of the magnitudes considered for the calculation of W: $u(s_\parallel) = s_\parallel - i \cdot a_\parallel$ is the displacement of the i-th vortex from the site of a perfect vortex chain with lattice spacing $a_\parallel = \langle a_i \rangle$, the average in a row. (d) Displacement correlator $W/a_\perp^2$ calculated along the transversal direction $s_\perp$ (statistics for 1,300 vortices in $Bi_2Sr_2CaCu_2O_{8+\delta}$ and 1,200 in $YBa_2Cu_3O_7$). Insert: Schematic representation on the magnitudes considered for the computation of W with $a_\perp = \langle a_j \rangle$, the average in a line. Fits of the displacement correlators with algebraic functions $A \cdot x^{2\zeta}$ (full lines) yield the roughening exponents 2ζ and factors A indicated in the legends. Error bars represent the standard deviation of data when averaging at a given q.

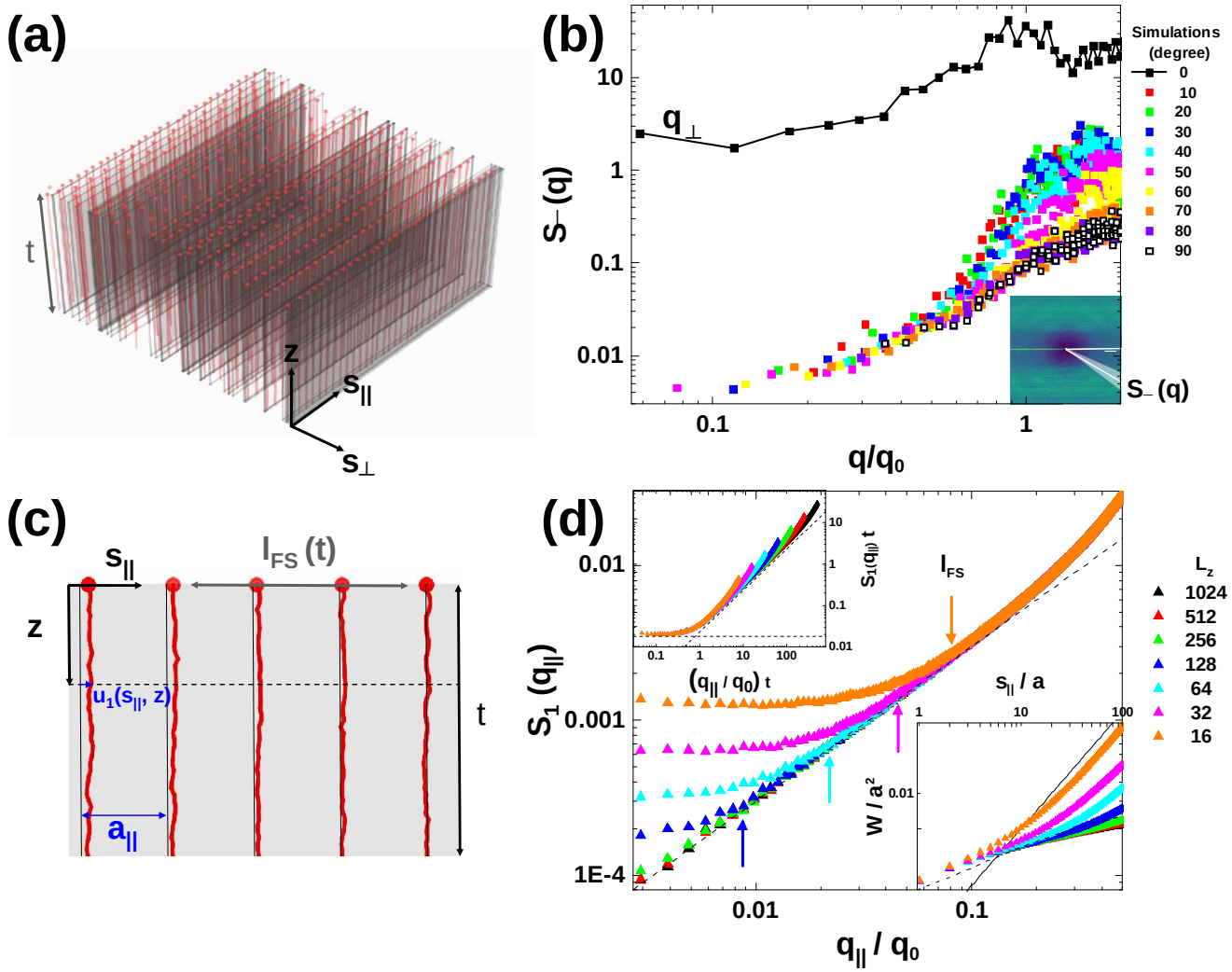


Figure 5: **Simulations of a structure of interacting elastic vortex lines in samples with planar defects.** (a) Snapshot of a quenched configuration obtained from three dimensional Langevin dynamics simulations of interacting vortices (red lines) in presence of parallel randomly-located PD (gray planes). Circles highlight vortex tips at the sample surface. The coordinate system and the thickness are indicated. (b) Angular structure factor $S_\theta(q)$ of the vortex positions at the sample surface for different angles θ indicated in the legend. The insert shows the $S(q_x, q_y)$ data considered to calculate the curves in the main panel. (c) Schematics of the planar vortex row model indicating the displacement field $u_1(s_\parallel, z)$, the average spacing $a_\parallel$ for a perfect row with the same vortex density, and the characteristic thickness-dependent crossover length $l_{\rm FS}$. (d) Results for the configurations of the planar vortex row at the surface of the sample ($z = 0$) for different sample thicknesses proportional to the number of layers in the simulation L_z. Main panel: $S_1(q_\parallel)$ structure factor for different sample thicknesses. The dashed black line is a linear function. Arrows indicate the crossover behavior at $q_\parallel/q_0 \sim 1/l_{\rm FS}$. Bottom-right insert: Displacement correlator as a function of the distance along the row $s_\parallel$. The full line is a linear function that reasonably describes the data in the large wavelength limit of thin samples whereas the dashed line is a logarithmic growth that follows the data at short wavelengths for thick enough samples. Top-left insert: Structure factor data $S_1(q_\parallel)t$ vs. $q_\parallel t$ showing a scaling collapse and the two regimes separated by the crossover wavevector, $2\pi/l_{\rm FS} \propto 2\pi/t$.